Tunable waveguide and cavity in a phononic crystal plate by controlling whispering-gallery modes in hollow pillars

Yabin Jin,[1,2] Nicolas Fernez,[2] Yan Pennec,[2,*] Bernard Bonello,[3] Rayisa P. Moiseyenko,[4] Stéphanie Hémon,[2] Yongdong Pan,[1] and Bahram Djafari-Rouhani[2]

[1]*School of Aerospace Engineering and Applied Mechanics, Tongji University, 100 Zhangwu Road, 200092, Shanghai, China*

[2]*Institut d'Electronique, de Microélectronique et de Nanotechnologie, Centre national de la recherche scientifique (CNRS), Unités mixtes de recherche (UMR) 8520, Université de Lille 1, 59650, Villeneuve d'Ascq, France*

[3]*CNRS, UMR 7588, Institut des NanoSciences de Paris, F-75005, Paris, France*

[4]*Department of Physics, Technical University of Denmark (DTU), Physics Building 309, DK-2800 Kongens Lyngby, Denmark*

(Received 6 November 2015; revised manuscript received 14 January 2016; published 12 February 2016)

We investigate the properties of a phononic crystal plate with hollow pillars and introduce the existence of whispering-gallery modes (WGMs). We show that by tuning the inner radius of the hollow pillar, these modes can merge inside both Bragg and low frequency band gaps, deserving phononic crystal and acoustic metamaterial applications. These modes can be used as narrow pass bands for which the quality factor can be greatly enhanced by the introduction of an additional cylinder between the hollow cylinder and the plate. We discuss some functionalities of these confined WGM in both Bragg and low frequency gaps for wavelength division in multiplexer devices using heteroradii pillars introduced into waveguide and cavity structures.

DOI: 10.1103/PhysRevB.93.054109

I. INTRODUCTION

Phononic crystals (PCs) [1–4], or acoustic band gap materials, constituted of a periodic arrangement of inclusions embedded in a matrix are receiving increasing attention for elastic/acoustic wave control and have found several fields of applications such as waveguiding [5,6], filtering [7], acoustic lensing [8–11], and fluid sensing [12]. Besides the two-dimensional (2D) infinite crystal and the control of bulk elastic waves, the interest of the phononic community has turned to the control of waves confined on the surface of a half-infinite PC [13,14] or propagating in finite PC plates. The latter geometry has been studied by considering either periodic inclusions [15,16] in particular holes, in a slab, or a periodic array of pillars on top of the plate [17,18]. It has been shown that the pillar structure exhibits two types of band gaps resulting either from Bragg scattering when the wavelength is in the order of the lattice parameter or from local resonances of the pillars at large wavelength [17,18]. It can then be described, respectively, as a PC or as an acoustic metamaterial. Because of this dual aspect, a great deal of work has been devoted to these structures, and different objectives have been pursued. Playing with the nature of the constitutive material, Oudich *et al.* [19] have shown the opening of very low resonant absolute band gaps in a plate covered with one or two layers of stubs made of soft rubber. Changing the geometry of the pillar, Hsu [20] investigated numerically the propagation of Lamb waves through an array of stepped resonators on a thin slab. Experimentally, Achaoui *et al.* [21] reported on the propagation of surface guided waves in a periodic arrangement of pillars on a semi-infinite medium. The negative properties of the low frequency modes have also been considered [22,23] for focalization applications. El Hassouani *et al.* [24] studied theoretically the simultaneous existence of phononic and photonic band gaps in a periodic array of silicon pillars deposited on a homogeneous thin silica plate for potential optomechanical applications. Finally, Davis and Hussein [25] introduced the concept of a locally resonant nanophononic metamaterial for thermoelectric energy conversion. Therefore, since the early papers in this topic [17,18], pillar structures have become a useful platform for many fundamental and applied investigations in the frame of PCs and acoustic metamaterials [6,26].

In this paper, we theoretically explore the existence and some functionalities of the pillar structure when the latter are constituted by hollow cylinders. Indeed, the hollow cylinders can display whispering-gallery modes (WGMs) whose quality factors can be greatly enhanced when the slab is separated from the hollow pillar by a second thin cylinder. Thus, the pillar is constituted by two layers, and the WGM confined in the upper layer interacts very weakly with the modes propagating in the slab. Let us mention that WGMs date back to the works of Rayleigh [27] in the field of acoustics, following the observation in St. Paul's Cathedral. The recent interest in the literature is about high Q optical WGM resonators, which can play a very significant role in photonics for applications in sensing [28] or photovoltaic [29]. Recent studies report the potentiality of these modes in the field of PC. Li *et al.* [30] immersed an isolated tube in liquid medium and showed that WGMs can exhibit a narrow periodic transmission dip with a high quality factor, while Kaproulias and Sigalas [31] considered the disk geometry for sensing application. The main recent interest in WGMs is related to the excitation of acoustic modes in optical WGM resonators via backward stimulated Brillouin scattering (SBS) [32,33]. In this context, acoustic WGMs have been recently investigated in spherical and cylindrical resonators within the theory of elasticity [34]. The displacement fields of the modes studied in this paper have similar shapes as the ones reported in those previous papers; hence the denomination of WGMs will be adopted here. As mentioned above, the novelty of the modes proposed here is their strong degree of confinement inside the pillars and a high quality factor hence allowing for several applications related

*Corresponding author: yan.pennec@univ-lille1.fr

to the manipulation of the acoustic waves such as guiding and filtering, both in the range of the Bragg and low frequency gaps.

In the first part of this paper, we present an analysis of the existence and behavior of the WGM in pillar structures. Then, the second part is devoted to discussing practical functionalities of these structures for filtering and multiplexing applications when waveguides and cavities with different hollow cylinders radii are inserted into the slab PC. We investigate the case of a homogeneous silicon plate with a square array of hollow pillars deposited on one side. The paper is organized as follows. In Sec. I, we calculate the dispersion of the elastic waves and their transmission through the structure, and we show the existence of WGMs and their tunability by modifying the inner radius of the hollow pillars. In Sec. II, we discuss the conception of a high resolved filter, tuning the WGM and improving the quality factor of the filter by introducing an additional thin cylinder at the basis of the hollow cylinder. Finally, in Secs. III and IV, we investigate waveguide and cavity capabilities and propose some designs of compact multiplexers with an appropriate distribution of inner radii in both Bragg and subwavelength ranges.

II. WHISPERING-GALLERY MODES

We consider a structure made of a square lattice of hollow pillars deposited on a thin homogeneous plate with a periodicity in the (x,y) plane. The z axis direction is chosen perpendicular to the plate. The elementary unit cell is presented Fig. 1 in which the geometrical parameters are the lattice constant a, the height h of the hollow pillars, and the thickness e of the plate. r and r_i correspond, respectively, to the outer and inner radius of the hollow pillar. The complete structure is made of silicon, assuming a cubic symmetry with the crystallographic axes oriented along the coordinate axes x, y, and z. The elastic constants are $C_{11} = 166\,\text{GPa}$, $C_{12} = 64\,\text{GPa}$, and $C_{44} = 79.6\,\text{GPa}$, and the mass density is $\rho = 2330\,\text{kg m}^{-3}$.

All dispersion and transmission curves have been computed using the finite element code COMSOL Multiphysics®. Periodic boundary conditions are applied on each side of the unit cell in the (x, y) plane. The dispersion and transmission

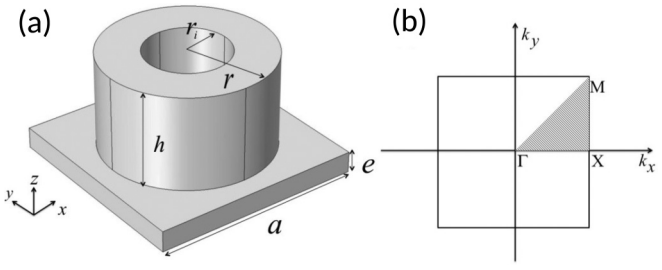

FIG. 1. (a) 3D-schematic view of the elementary unit cell constituting the PC made of finite hollow pillars deposited on a thin homogeneous plate. The lattice constant is a, and the thickness of the plate is e. The hollow pillar has a height h and an inner and outer radius, respectively, denoted r_i and r. (b) Periodic boundary conditions are applied in the (x, y) plane on each side of the unit cell, constituting a periodic crystal with a square array symmetry for which the first Brillouin zone and its irreducible part is presented.

curves will be presented as a function of the reduced frequency, $\Omega = \omega a/(2\pi v_t)$, where $v_t = 5844\,\text{m s}^{-1}$ is the transverse bulk velocity of silicon along x.

Before presenting the results for the hollow pillars on plate, we have calculated as a reference the band structure of the native PC containing filled cylinders of silicon ($r_i = 0$). The choice of the geometrical parameters is done in order to obtain two wide absolute band gaps, one at the Bragg frequency regime and the second in the low frequency range [17]. In Fig. 2(a), we present the dispersion curves calculated along the direction ΓX of the Brillouin zone with $e/a = 0.1$, $h/a = 0.55$, and $r/a = 0.42$. With this set of parameters, we obtain two wide absolute band gaps around the respective reduced frequency 0.2 (red area) and 0.6 (blue area). The low frequency band gap is due to the local resonances of the pillars [17] at a wavelength almost 10 times larger than the lattice constant a. The Bragg gap comes from the periodicity of the crystal and the collective scattering effects between the pillars. These reduced geometrical parameters (e/a, h/a, and r/a) will be kept fixed in the rest of the paper.

Figure 2 shows the evolution of the dispersion curves as a function of the inner radius. The introduction of the hollow cylinders gives rise to two new dispersion branches labeled 1 and 2 that do not exist in the native PC. By increasing r_i/a from 0 to 0.35, they move towards lower frequencies.

At $r_i/a = 0.145$ [Fig. 2(b)], the two branches appear inside the Bragg gap, while the gap boundaries and the branches below are almost unaffected. When increasing r_i/a to 0.25 [Fig. 2(c)], the two branches cross the lower edge of the Bragg gap, and the branch labeled 1 interacts with the Lamb waves situated just below the reduced frequency 0.40. For higher values of r_i/a, the two branches still move downward while new modes progressively appear at higher frequencies. At higher r_i/a (not shown), the Bragg gap gets closed. For $r_i/a = 0.30$ to 0.35, the frequencies of the two branches continue decreasing and cross the low frequency gap. However, at these low frequencies, the modes interact with the Lamb waves of the plate and do not give rise to isolated branches, as was the case in the Bragg gap. We see in the next section how to make them flat by a better confinement of the modes and therefore make the structure useful for both PC and acoustic metamaterial applications.

Despite the fact that these branches are slightly dispersive due to their interaction with the Lamb waves in the plate, they still remain nearly flat (i.e., with a small group velocity), and one can recognize that they are essentially WGMs of the hollow cylinders, as shown in the displacement field maps of Fig. 3(a) corresponding to $r_i/a = 0.145$. For such modes, the acoustic path around the hollow pillar should be a multiple integer of the wavelength, here equal to 2 for both modes. Figure 3(b) represents a top view of the component U_z of the displacement field. It brings to light the main difference between the two modes that explain the existence of two separates frequencies. While mode 2 is almost totally confined inside the hollow pillar, mode 1 strongly interacts with the four first neighbors hollow cylinders of the unit cell via the plate.

Although the modes studied here have a quadrupolar shape, we have also identified higher frequency modes with hexapolar or octopolar symmetries that fall outside the band gap. Let us mention that modes with dipolar or quadrupolar

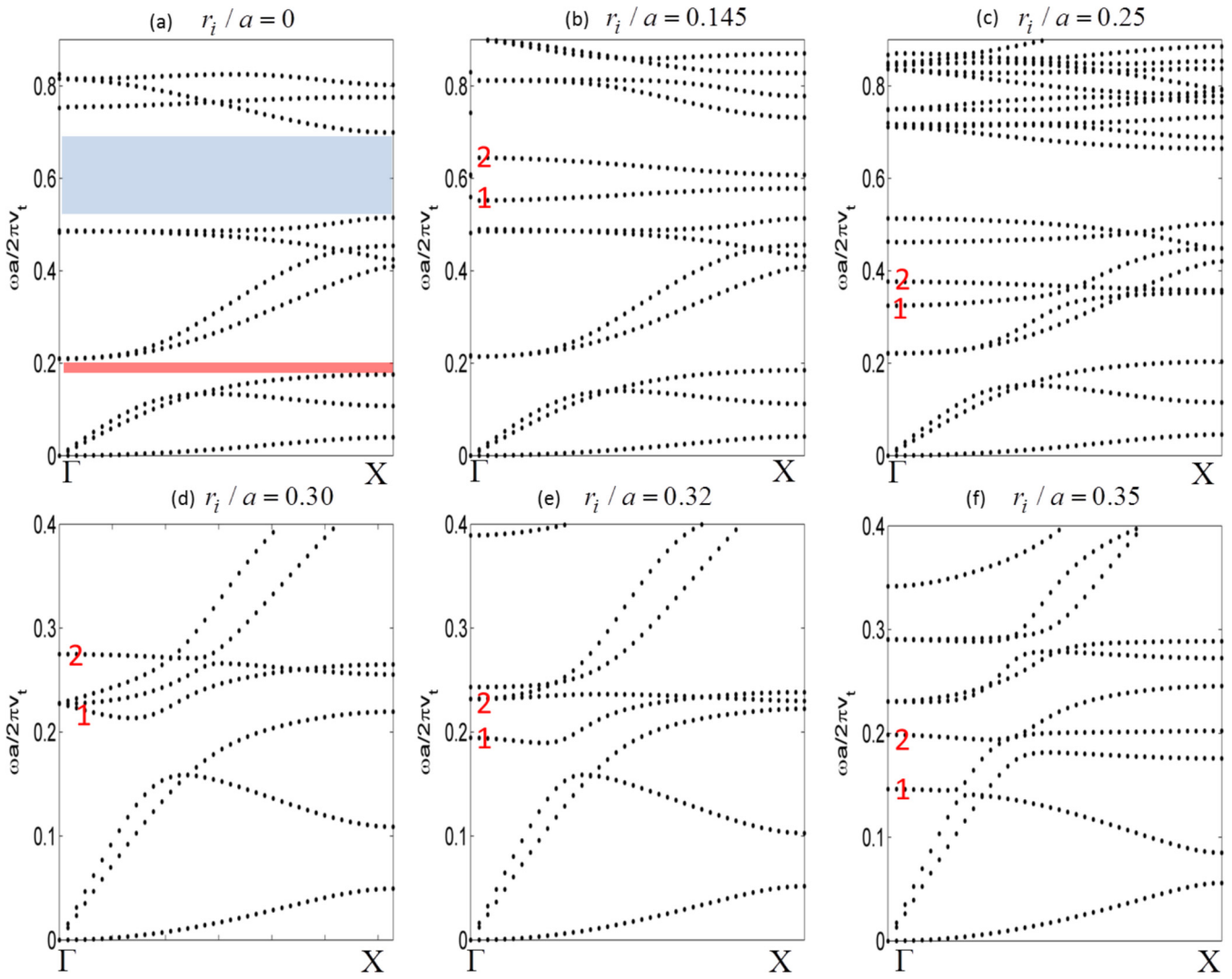

FIG. 2. Dispersion curves of the hollow pillars on a thin silicon plate in the ΓX direction of the first irreducible Brillouin zone in two reduced frequency ranges ([0; 0.9] for (a), (b), (c) and [0; 0.4] for (d), (e), (f)) with different inner radii (a) $r_i/a = 0$, (b) $r_i/a = 0.145$, (c) $r_i/a = 0.25$, (d) $r_i/a = 0.30$, (e) $r_i/a = 0.32$, (f) $r_i/a = 0.35$. The thickness of the plate is $e/a = 0.1$, the outer radius $r/a = 0.4$, and the height $h/a = 0.45$. The hatched areas correspond to the low (red) and Bragg (blue) absolute band gaps of the native crystal. The 1 and 2 branches come from the hollow pillar structure.

symmetries have also been studied in other context of acoustic metamaterials [35]. We have also compared the frequencies and shapes of the WGMs with those obtained when the pillars are almost isolated from each other, namely by assuming a period 10 times higher than it is in the above calculations. It is found that the results are insensitive to the pillar separation, not only for quadrupolar but also for higher hexapolar or octopolar modes. Of course, the resonance frequencies will change if the membrane at the bottom of the pillar is removed because, depending on the WGM, its displacement field is more or less affected by the presence of the membrane.

Figure 3(c) summarizes the behavior of the two WGMs as a function of the inner radius of the hollow pillar. Both of the WGMs' frequencies decrease as the inner radius increases. This behavior can be understood when noticing that higher values of the average radius $\langle r \rangle = (r + r_i)/2$ increases the acoustic path along the perimeter $2\pi\langle r \rangle$ of the cylinder. As a result, when $r_i/a = 0.145$ (resp. 0.35), the whispering eigenmodes 1 and 2 fall in the middle of the Bragg (resp. low frequency) gap.

In order to show the filtering capacity of the structure based on WGMs, we calculate the transmission spectrum through a finite PC plate containing five rows of hollow pillars. Perfect matching layers (PMLs) are applied at the entrance and the exit of the slab to avoid any reflections from the external edges. Periodic boundaries conditions are applied along y direction on each side of the unit cell. The incident wave is the A_0 Lamb wave of the plate, propagating along the x axis, and launched by applying a harmonic displacement U_z in the (y, z) plane in front of the crystal. To determine the transmission coefficient, the displacement field is recorded in the far field behind the PC and then normalized to the displacement field propagating in the homogeneous plate.

As stated above, the choice of $r_i/a = 0.145$ appears as the best because of the frequencies of the WGMs being in the center of the Bragg gap. We represent in Fig. 4 the

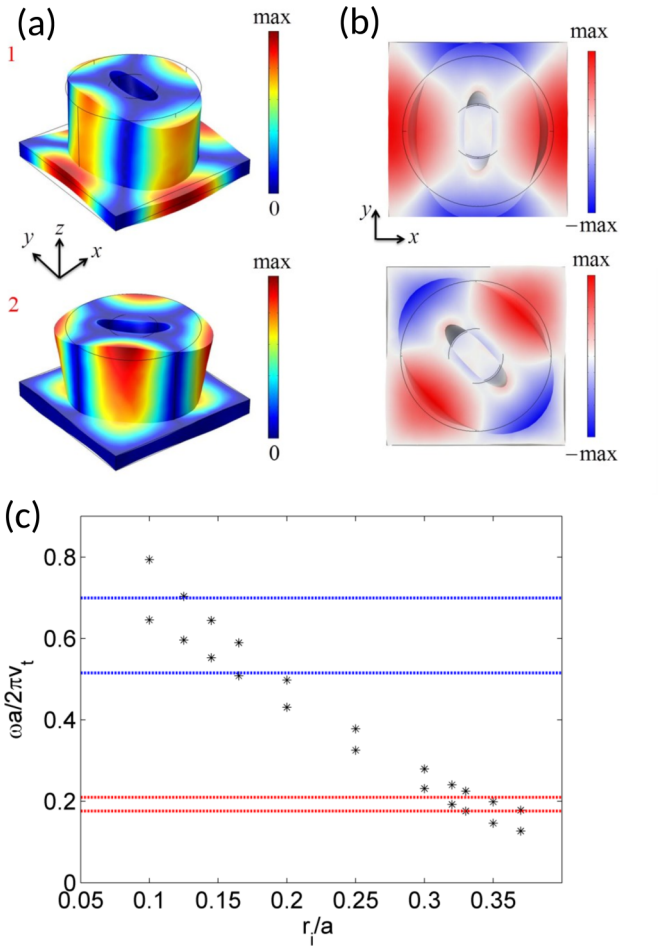

FIG. 3. (a) Representation of the displacement field distribution and the deformation of the unit cell at the frequency of WGMs 1 and 2 at the Γ point for $r_i/a = 0.145$. (b) Top view representation of the component U_z of the displacement field for the two modes. (c) Evolution of the frequency of mode 1 and 2 as a function of the inner radius r_i of the hollow pillar. The blue (resp. red) dashed lines represent the boundaries limits of the Bragg (resp. low frequency) band gap.

transmission coefficient as a function of frequency, together with the dispersion curves. One can notice a relatively narrow transmission peak associated with WGM 1, while WGM 2 does not transmit. This result can be understood on the basis of symmetry consideration. Indeed, the incident wave A_0 is symmetric with respect to the symmetry plane $\Pi(x, z)$. Thus, it can only excite WGM 1, which has the same symmetry, and not WGM 2, which is antisymmetric with respect to this plane. Then, the latter appears as a deaf band [36,37] in the transmission spectrum.

III. WGMS WITH HIGH QUALITY FACTOR AND NARROW BAND FILTERING

In the previous section, we have shown that WGMs can be used as a tunable band filter in the Bragg and low frequency band gaps of the PC. In this section, we shall show how the quality factor of the WGM-based transmitted wave can be significantly increased. Indeed, the width of the transmission

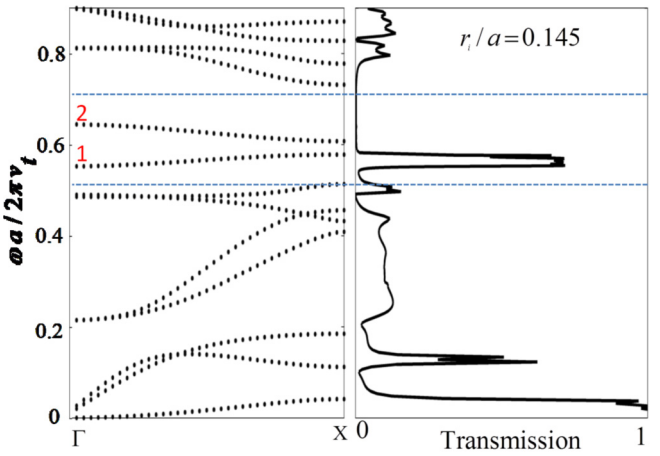

FIG. 4. Dispersion curve (left) and transmission spectrum of the antisymmetric Lamb wave (right) through the hollow cylinder PC with inner radius $r_i/a = 0.145$. The blue dashed lines represent the boundaries of the Bragg gap.

peak, or accordingly the width of the narrow band associated with WGM 1 in Fig. 4, are related to its interaction with the Lamb waves of the plate, as can be seen from the maps of the displacement field (Fig. 3). To enhance the confinement of the WGM without changing significantly the associated field, we insert a silicon solid cylinder of height l at the basis of the hollow pillar [see the red block in the inset of Fig. 5(a)].

We show in Fig. 5(b) the dispersion curves in the range [0.4; 0.8] as a function of the reduced height l/h of the added cylinder when $h/a = 0.45$. We can observe that the two branches associated to the WGMs become more and more flat as l/h increases, which is the signature of a better confinement of the modes inside the unit cell. To quantify the role of the added cylinder on the pass band, we have calculated the quality factor $Q = f/\Delta f$, where f is the central frequency of the pass band and Δf the full width at half maximum of the transmission peak. Figure 5(a) shows a significant increase in the quality factor with increasing the reduced height l/h. For $l/h = 0.64$, the quality factor reaches $Q = 280$, i.e. more than 10 times the value obtained without the additional cylinder, paving the way to a high resolved narrow pass band device for filtering applications.

Increasing now the inner radius to $r_i/a = 0.35$, we shift the two WGMs in the vicinity of the low frequency band gap. As previously, we insert the silicon solid cylinder of height l at the basis of the hollow pillar. Figure 5(c) represents the dispersion curve in the low frequency regime for $l/a = 0$, 0.22, and 0.44. One can see that when l/h increases, the interaction of the branches 1 and 2 with the Lamb modes decreases, reaching finally to a localization of the two WGMs in the middle of the narrow low frequency band gap when $l/h = 0.54$.

IV. MULTIPLEXING DEVICES BASED ON TUNABLE WAVEGUIDES AND CAVITIES

As reported in Fig. 3(c), the position of the narrow pass band is very sensitive to the inner radius of the hollow pillar.

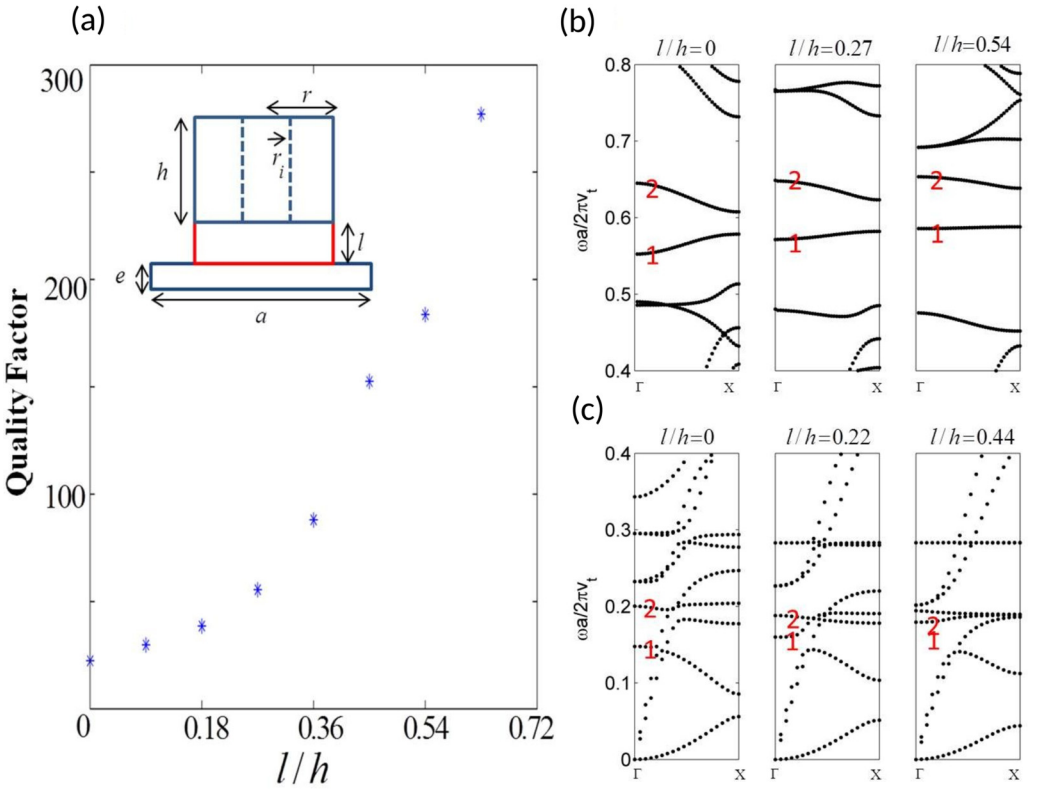

FIG. 5. (a) (Inset) Schematic cross section of the unit cell with the added full silicon cylinder of height l (red block) with $h/a = 0.45$, $e/a = 0.1$, and $r/a = 0.4$. (Graph) Evolution of the quality factor of the narrow pass band based on the WGM 1 as a function of l/h, ($r_i/a = 0.145$). (b) Dispersion curves magnified in the Bragg gap range ([0.4; 0.8]) for different value of l/h. (c) Dispersion curves magnified in the low frequency gap range ([0; 0.4]) for different value of l/h.

Actually, the narrow pass band can cover the full Bragg gap (i.e., the reduced frequency range [0.55, 0.7]) when r_i/a is varied from 0.145 to 0.155. For a mixed system composed of different inner radii, different narrow pass bands inside the Bragg gap are expected. We propose to use this property for the design of a new kind of mono- and multichannel wavelength division multiplexers by inserting appropriate waveguides and cavities in a PC slab. A similar property was earlier proposed in a 2D PC constituted by hollow cylinders filled with different liquids [38]. For the sake of computational convenience, the height of the added cylinder is fixed to $l/a = 0.2$ ($l/h = 0.36$) in the following calculations, leading to a Q factor of 100.

A. Multichannel wavelength multiplexer

We first consider [inset of Fig. 6(a)] a (5×5) supercell with periodic conditions along y axis and PML in the direction of propagation x. The phononic plate contains two linear waveguides separated from each other by one row of filled cylinders to prevent significant leakage between the guides. The waveguides are constituted by two rows of hollow pillars with the radius $r_i^{(a)}/a = 0.145$ and $r_i^{(b)}/a = 0.160$ for the waveguides a and b, respectively. We probe the transmission of the waveguides by launching the A_0 Lamb wave in front of the PC. The transmission spectrum, displayed in Fig. 6(a), features two narrow pass bands occurring at the reduced frequencies 0.543 and 0.581, inside the band gap. These values significantly differ from those obtained with the perfect hollow pillar phononic plate [Fig. 3(c)]. This means that the effect of confinement inside the waveguide on the transmission peak is far from being negligible while the narrowness of

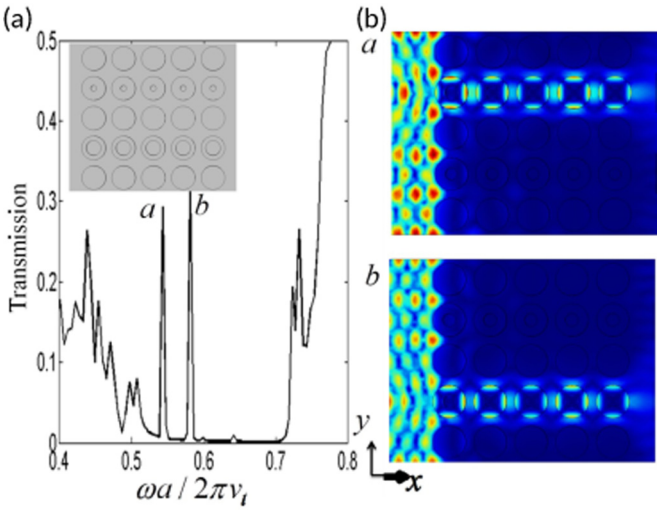

FIG. 6. (a) (Inset) Schematic representation of the multichannel wavelength multiplexer. (Graph) Transmission spectrum of the antisymmetric Lamb wave when the radius of the hollow pillars inside waveguide a and b are $r_i^{(a)}/a = 0.145$ and $r_i^{(b)}/a = 0.160$. (b) Displacement field distributions at the frequency of the two narrow pass bands a and b.

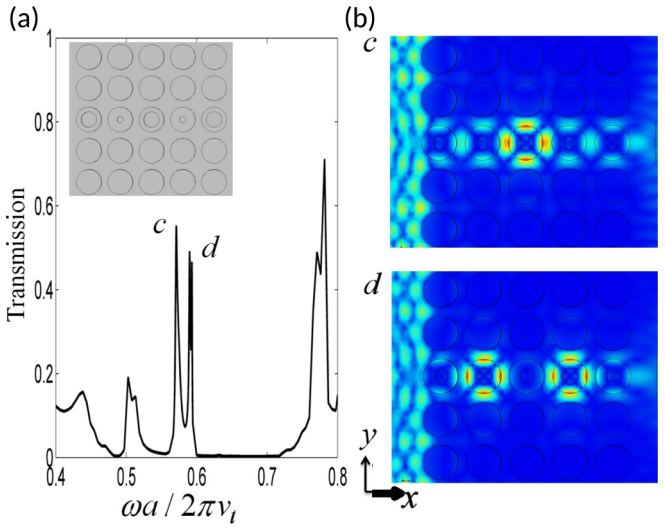

FIG. 7. (a) (Inset) Schematic representation of the monochannel wavelength multiplexer. (Graph) Transmission spectrum of the antisymmetric Lamb wave when consecutive hollow pillars inside the waveguide have radii of $r_i{}^{(c)}/a = 0.145$ and $r_i{}^{(d)}/a = 0.140$. (b) Displacement field distributions at the frequency of the two narrow pass bands c and d.

the pass bands is preserved. As seen in the displacement field distributions of Fig. 6(b), the two narrow pass bands correspond respectively to the transmitted wave through the waveguide a and b. We then have created a multichannel wavelength multiplexer.

B. Monochannel wavelength multiplexer

Next, we consider the propagation at the frequencies of two narrow passbands through one single waveguide composed of alternating hollow cylinders with two different radii [see inset in Fig. 7(a)] of $r_i{}^{(c)}/a = 0.145$ and $r_i{}^{(d)}/a = 0.140$. The transmission spectrum is presented Fig. 7(a) in which one can see the occurrence of two narrow passbands at the reduced frequencies $f^{(c)} = 0.571$ and $f^{(d)} = 0.590$. This means that it becomes possible to transport two different wavelengths through the same channel. The elastic wave transmission comes from evanescent waves inside the slab, which in turn allows for the overlapping of the elastic fields between two next nearest neighbors hollow pillars with identical radii. The waveguide then allows for the tunneling and, therefore, to the propagation of the elastic wave. Figure 7(b) sketches the displacement field at the frequencies $f^{(c)}$ and $f^{(d)}$, where the enhancement of the fields inside the hollow pillars is clearly observable for both radii.

C. Compact multiplexer based on linear cavity

Another way to obtain high-Q resonators is to create an infinite linear cavity oriented perpendicularly to the direction of propagation [39]. The inset of Fig. 8(a) shows the unit cell of a periodic structure that contains two lines of hollow pillars surrounded from each side by one line of solid cylinders. The unit cell has a finite size along the x axis and is periodic in the y direction. The cavity is constituted by two different hollow

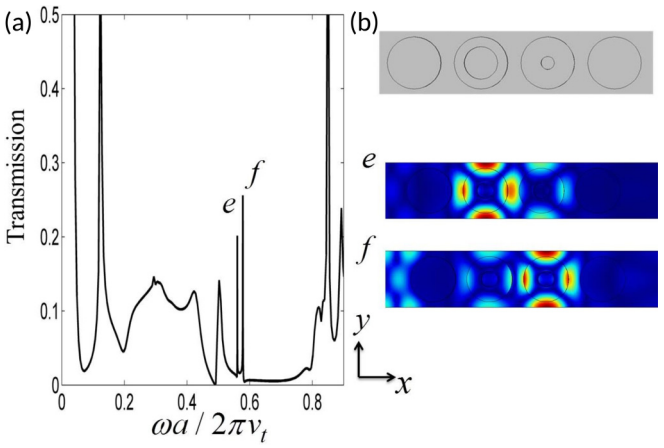

FIG. 8. (a) (Inset) Schematic representation of the compact wavelength cavity multiplexer. (Graph) Transmission spectrum of the antisymmetric Lamb wave when the radius of the hollow pillars inside waveguide are $r_i{}^{(e)}/a = 0.145$ and $r_i{}^{(f)}/a = 0.140$. (b) Displacement field distributions at the frequency of the two narrow pass bands e and f.

pillars with respective radii $r_i/a^{(e)} = 0.145$ and $r_i/a^{(f)} = 0.140$. The transmission of the antisymmetric Lamb wave launched in the x direction and presented in Fig. 8(a) shows that the structure supports two narrow pass bands at $f^{(e)} = 0.561$ and $f^{(f)} = 0.578$, respectively [Fig. 8(b)]. Note that the confinement of the elastic energy is achieved by using only one PC layer embedding the cavity region and leading to an extremely compact multiplexer filter with high Q factor.

V. SUBWAVELENGTH WAVEGUIDE

This last section deals with an application of the WGMs inside the low frequency band gap. As established previously, the two modes can be localized inside the narrow low frequency band gap as far as we chose a large inner radius ($r_i/a = 0.35$). The second condition is to add a solid silicon

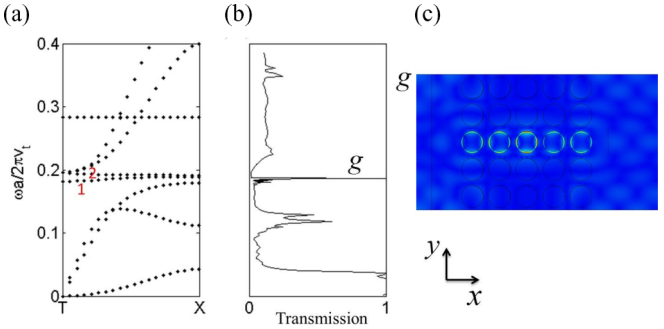

FIG. 9. (a) Dispersion curve in the low frequency range [0; 0.4] corresponding to the perfect PC made of hollow pillars on plate with the set of geometrical parameters $r_i/a = 0.35$, $l/h = 0.49$, $h/a = 0.45$, $r/a = 0.4$, and $e/a = 0.1$. (b) Transmission spectrum of the antisymmetric Lamb wave through the waveguide of hollow pillars inserted inside a full silicon pillar crystal. (c) Displacement field distributions at the reduced frequency 0.19 corresponding to the narrow pass bands g.

cylinder of thickness $l/h = 0.49$ between the hollow pillar and the plate to get the dispersion branches almost flat. Under these conditions and the set of other geometrical parameters $h/a = 0.45$, $r/a = 0.4$, and $e/a = 0.1$, we have obtained the dispersion curve of the perfect PC made of hollow pillars on plate presented Fig. 9(a). We then built the design of the subwavelength waveguide by replacing one row of the perfect PC with hollow pillars. The transmission spectrum of the antisymmetric Lamb wave depicted in Fig. 9(b) shows the transmission of a very narrow peak at the reduced frequency 0.19. As seen in Fig. 9(c), the transmission comes from the excitation of the WGM 1 on top of the hollow cylinders.

VI. CONCLUSIONS

We theoretically investigated the vibration properties of a PC plate with hollow pillars on top. The computed dispersion curves show the occurrence of two new branches of dispersion that do not appear in the native PC. These branches originate from the excitation of WGMs circulating around the upper boundary of the hollow pillar. By changing the inner radius of the hollow cylinder, we have been able to tune the frequencies of the WGMs inside the Bragg band gap. Through the computation of the transmission coefficient of an antisymmetric Lamb wave, we have shown that one of the WGMs gives rise to a transmitted pass band that can be used as a filter. The quality factor of the filter has been further improved by inserting a solid cylinder in between the plate and the hollow pillar. We then applied the high resolved filter to different kind of multiplexers, based on multichannel or monochannel waveguides or cavity. We also showed that the WGMs can reach the low frequency range, adding a new type of elastic field localization inside the resonators, with the opportunity to perform interactions with the existing low frequency band gap. The demonstration of an efficient subwavelength waveguide with high quality factor has been done. We believe that this structure will pave the way to future new physical behaviors for PC and acoustic metamaterials by changing the nature of the constitutive elements or filling the hollow cylinders with liquids, rubber, or other core-shell elements. The investigations and achievements of these PC resonator structures will show the possibility to build acoustic sensors, filters, and acoustic resonators working with improved performances that makes them excellent candidates for wireless communication and sensing applications.

ACKNOWLEDGMENTS

This paper was supported by the Agence Nationale de la Recherche (ANR) and the Direction Générale de l'Armement (DGA) under the project Metactif, Grant No. ANR-11-ASTR-015. Yabin Jin acknowledges a scholarship provided by China Scholarship Council No. 201406260170.

[1] M. S. Kushwaha, P. Halevi, L. Dobrzynski, and B. Djafari-Rouhani, Phys. Rev. Lett **71**, 2022 (1993).
[2] M. Sigalas and E. N. Economou, Solid. State. Commun **86**, 141 (1993).
[3] A. Khelif and A. Adibi, *Phononic Crystals: Fundamentals and Applications* (Springer-Verlag, New York, 2015).
[4] Y. Pennec, J. O. Vasseur, B. Djafari-Rouhani, L. Dobrzyński, and P. A. Deymier, Surf. Sci. Rep **65**, 229 (2010).
[5] M. Kafesaki, M. M. Sigalas, and N. Garcia, Phys. Rev. Lett. **85**, 4044 (2000).
[6] P. Celli and S. Gonella, Appl. Phys. Lett **107**, 081901 (2015).
[7] T. T. Wu, L. C. Wu, and Z. G. Huang, J. Appl. Phys. **97**, 094916 (2005).
[8] C. Qiu, Z. Liu, J. Mei, and J. Shi, Appl. Phys. Lett. **87**, 104101 (2005).
[9] S.-C. S. Lin, T. J. Huang, J.-H. Sun, and T.-T. Wu, Phys. Rev. B **79**, 094302 (2009).
[10] J. Zhao, B. Bonello, R. Marchal, and O. Boyko, New J. Phys. **16**, 063031 (2014).
[11] Y. Jin, D. Torrent, Y. Pennec, Y. Pan, and B. Djafari-Rouhani, J. Appl. Phys. **117**, 244904 (2015).
[12] S. Amoudache, Y. Pennec, B. Djarafi-Rouhani, A. Khater, R. Lucklum, and R. Tigrine, J. Appl. Phys **115**, 134503 (2014).
[13] T. T. Wu, Z. G. Huang, and S. Lin, Phys. Rev. B **69**, 094301 (2004).
[14] A. Khelif, Y. Achaoui, S. Benchabane, V. Laude, and B. Aoubiza, Phys. Rev. B **81**, 214303 (2010).
[15] A. Khelif, B. Aoubiza, S. Mohammadi, A. Adibi, and V. Laude, Phys. Rev. E **74**, 046610 (2006).
[16] J. O. Vasseur, A. C. Hladky-Hennion, B. Djafari-Rouhani, F. Duval, B. Dubus, Y. Pennec, and P. A. Deymier, J. Appl. Phys **101**, 114904 (2007).
[17] Y. Pennec, B. Djafari-Rouhani, H. Larabi, J. O. Vasseur, and A. C. Hladky-Hennion, Phys. Rev. B. **78**, 104105 (2008).
[18] T. T. Wu, Z. G. Huang, T. C. Tsai, and T. C. Wu, Appl. Phys. Lett **93**, 111902 (2008).
[19] M. Oudich, Y. Li, B. M. Assouar, and Z. Hou, New J. Phys. **12**, 083049 (2010).
[20] J. C. Hsu, J. Phys. D: Appl. Phys **44**, 055401 (2011).
[21] Y. Achaoui, A. Khelif, S. Benchabane, L. Robert, and V. Laude, Phys. Rev. B **83**, 104201 (2011).
[22] M. Oudich, B. Djafari-Rouhani, Y. Pennec, M. B. Assouar, and B. Bonello, J. Appl. Phys. **116**, 184504 (2014).
[23] V. E. Gusev and O. B. Wright, New J. Phys. **16**, 123053 (2014).
[24] Y. El Hassouani, C. Li, Y. Pennec, E. H. El Boudouti, H. Larabi, A. Akjouj, O. Bou Matar, V. Laude, N. Papanikolaou, A. Martinez, and B. Djafari Rouhani, Phys. Rev. B **82**, 155405 (2010).
[25] B. L. Davis and M. I. Hussein, Phys. Rev. Lett. **112**, 055505 (2014).
[26] M. Rupin, F. Lemoult, G. Lerosey, and P. Roux, Phys. Rev. Lett **112**, 234301 (2014).
[27] L. Rayleigh, Philos. Mag. **20**, 1001 (1910); **27**, 100 (1914).
[28] M. R. Foreman, J. D. Swaim, and F. Vollmer, Adv. in Opt. Photon **7**, 168 (2015).
[29] J. Grandidier, D. M. Callahan, J. N. Munday, and H. A. Atwater, Adv. Mater **23**, 1272 (2011).

[30] F. Li, M. Xuan, Y. Wu, and F. Bastien, Sensor. Actuat A: Phys. **189**, 335 (2013).
[31] S. Kaproulias and M. M. Sigalas, AIP Adv. **1**, 041902 (2011).
[32] L. Ding, C. Baker, P. Senellart, A. Lemaitre, S. Ducci, G. Leo, and I. Favero, Phys. Rev. Lett. **105**, 263903 (2010).
[33] M. Tomes and T. Carmon, Phys. Rev. Lett. **102**, 113601 (2009).
[34] B. Sturman and I. Breunig, J. Appl. Phys. **118**, 013102 (2015).
[35] Ying Wu, Yun Lai, and Zhao-Qing Zhang, Phys. Rev. B **76**, 205313 (2007); Yun Lai, Ying Wu, Ping Sheng, and Zhao-Qing Zhang, Nat. Mat. **10**, 620 (2011).
[36] J. V. Sánchez-Pérez, D. Caballero, R. Martinez-Sala, C. Rubio, J. Sánchez-Dehesa, F. Meseguer, J. Llinares, and F. Gálvez, Phys. Rev. Lett. **80**, 5325 (1998).
[37] V. Laude, R. P. Moiseyenko, S. Benchabane, and N. F. Declercq, AIP Adv. **1**, 041402 (2011).
[38] Y. Pennec, B. Djafari-Rouhani, J. O. Vasseur, A. Khelif, and P. A. Deymier, Phys. Rev. E. **69**, 046608 (2004).
[39] S. Mohammadi, A. A. Eftekhar, W. D. Hunt, and A. Adibi, Appl. Phys. Lett, **94**, 051906 (2009).